Computer simulation of the KvAP voltage-gated potassium channel: steered molecular dynamics of the voltage sensor

Luca Monticelli[a,b], Kindal M. Robertson[a], Justin L. MacCallum[a], D. Peter Tieleman[a,*]

[a] *Department of Biological Sciences, University of Calgary, 2500 University Dr. NW, Calgary, AB, Canada T2N 1N4*
[b] *Centre for Biomolecular Interdisciplinary Studies and Industrial Applications (CISI), University of Milan, Via Venezian, 21, 20133 Milan, Italy*

Received 21 December 2003; accepted 23 February 2004

First published online 18 March 2004

Edited by Fritz Winkler and Andreas Engel

Abstract The recent crystal structures of the voltage-gated potassium channel KvAP and its isolated voltage-sensing 'paddle' (composed of segments S1–S4) challenge existing models of voltage gating and raise a number of questions about the structure of the physiologically relevant state. We investigate a possible gating mechanism based on the crystal structures in a 10 ns steered molecular dynamics simulation of KvAP in a membrane-mimetic octane layer. The structure of the full KvAP protein has been modified by restraining the S2–S4 domain to the conformation of the isolated high-resolution paddle structure. After an initial relaxation, the paddle tips are pulled through the membrane from the intracellular to the extracellular side, corresponding to a putative change from closed to open. We describe the effect of this large-scale motion on the central pore domain, which remains largely unchanged, on the protein hydrogen-bonding network and on solvent. We analyze the motion of the S3b–S4 portion of the protein and propose a possible coupling mechanism between the paddle motion and the opening of the channel. Interactions between the arginine residues in S4, solvent and chloride ions are likely to play a role in the gating charge.

Key words: Non-equilibrium molecular dynamics; Molecular modeling; Potassium channel; Voltage gating; Shaker; Membrane protein

1. Introduction

Voltage-gated potassium (Kv) channels are a key component underlying electrical signaling in the nervous system. Since the cloning of the prototypical family member, Shaker [1], Kv channels have been probed exhaustively by a wide range of both experimental [2,3] and computational methods [4,5], including electrophysiological recording, scanning mutagenesis, site-specific accessibility studies, crosslinking, structural studies and molecular modeling. The general goal of all this work is to understand how these proteins are able to generate electrical signals in response to changes in the membrane potential.

Kv channels are tetrameric proteins, consisting of a central pore (helices S5 and S6, P loop and a cation-specific selectivity filter region) which is conserved among all potassium channels and of a voltage sensor (helices S1–S4, in particular helix S4), which is specific to voltage-gated channels [6]. In the past five years crystal structures of KcsA [7,8], MthK [9] and KirBac [10] have provided detailed structural information on the pore domain of potassium channels. Recently, a bacterial voltage-gated potassium channel (KvAP from the hyperthermophilic archaebacterium *Aeropyrum pernix*) was identified, cloned, and characterized [11], and the structure of its transmembrane domain determined. In addition, a separate structure of the isolated voltage-sensing domain consisting of helices S1–S4 was solved at 1.9 Å resolution [12].

These structures present several unexpected features, one of the most surprising of which is the location and orientation of the S4 helix. This helix contains five highly conserved arginine residues and is known to be crucial for the voltage-dependent gating [3,6]. In most models this helix was assumed to be oriented parallel to the channel axis, enclosed in a protein 'sleeve' that allows sliding of S4 up and down in response to changes in the membrane potential (see Fig. 1B). For example, a recent model of Shaker has S1–S4 as parallel transmembrane helices where S4 faces the groove between the S5/S6 helix of an adjacent monomer [13]. In the KvAP crystal structure, S4 lies perpendicular to the channel axis, at the periphery of the channel, and is fully exposed to the aqueous intracellular environment. Based on the crystal structure of KvAP, Jiang et al. have suggested a simple and elegant alternative mechanism for voltage activation in Kv channels. In this mechanism, S4 and part of S3 constitute a so-called paddle, which rotates and crosses the whole membrane in response to membrane depolarization (Fig. 1C) [14].

Several recent reviews have pointed out however that the location and structure of S1–S4 at first sight appear to be inconsistent with a significant body of experimental data on voltage-gated channels [13,15,16]. We will not repeat those arguments in detail here, but would like to single out five points. First, there is a significant difference between the S1–S4 domain in the full KvAP structure and in the isolated paddle structure. Second, when the S5–S6 domain is used to estimate where the membrane would be (the structure was solved in detergent), the S1–S4 domain would be located in the cytosolic solution, in what would be a closed conformation of the channel. Third, much of the experimental data that appear inconsistent with the KvAP structure show that the linker between S3 and S4 is accessible, at least in Shaker, from the extracellular side regardless of the conformation of the channel [13,17,18]. This may be partially reconciled by the additional residues present in the S3–S4 linker of Shaker

*Corresponding author. Fax: (1)-403-289-9311;
Web: http://moose.bio.ucalgary.ca.
E-mail address: tieleman@ucalgary.ca (D.P. Tieleman).

0014-5793/04/$30.00
doi:10.1016/S0014-5793(04)00271-6

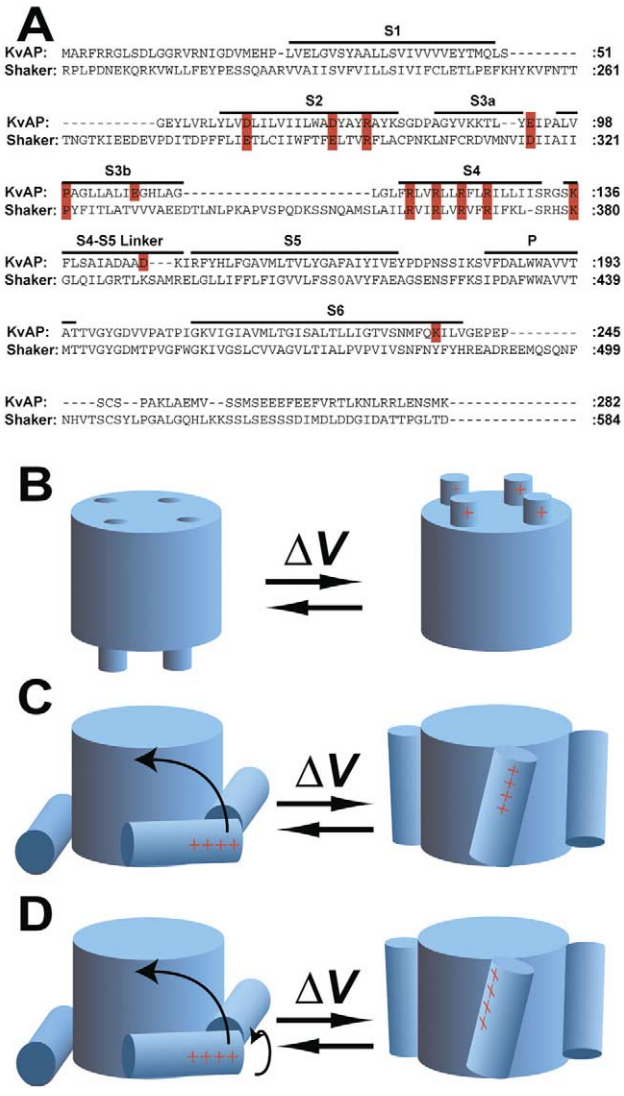

Fig. 1. A: Sequence alignment of KvAP and Shaker [12]. B: Schematic representation of the motion of S4 according to the conventional model, C: to the model proposed by Jiang et al. [12], and D: to motions observed in the MD simulation in this paper.

that are not present in KvAP and do not appear necessary for function [19]. Fourth, the location of the S1–S4 helices is such that several charges are exposed in the membrane, and S4 is facing the lipids. Fifth, the proposed movement of the paddle is quite large, but several spectroscopic studies have suggested that the movement of S4 during voltage activation is quite limited in space [20,21]. The first two points are probably related to crystallization conditions and to the presence of FAB antibodies, bound to the tip of each paddle.

In this paper, we describe a steered molecular dynamics (MD) simulation of a model of KvAP built by combining the high-resolution structure of the isolated paddle with the full protein structure. We follow the dynamics of the model as we pull the paddles through the membrane and investigate some of the possible coupling mechanisms between the motion of the voltage sensors and the opening of the pore. By placing KvAP in a more realistic membrane environment and modeling the high-resolution paddle structure into the full protein we can to some degree address the first two points. By pulling the paddles up we also obtain an approximate model of an open channel based on the crystal structure, which can be compared to the experimental data. We can also gain insight into which residues are lipid exposed during this process.

2. Materials and methods

2.1. Simulation setup

The crystallographic structure of the full KvAP protein (PDB code: 1ORQ) was used as a starting structure for our simulations. The protein was embedded in a three-layer box (water/octane/water) that mimics the membrane environment; the thickness of the octane layer was approximately 3 nm (the thickness of the hydrophobic core of a 'typical' membrane) in the proximity of the protein. Ionization states of the protein side chains were the same as the standard at pH 7 for each residue, and the total charge on the protein was zero. Potassium and chloride ions replaced 26 water molecules. The system consisted of 1477 octane molecules, 24 823 water, 13 potassium and 13 chloride ions, and the size of the simulation box was $11.7\times11.7\times9.2$ nm.

The system was energy minimized with a steepest descent method for 500 steps, followed by solvent equilibration in a 200 ps MD run with position restraints on the protein backbone. The force constant on the protein atoms was 1000 kJ mol^{-1} nm^{-2}. The solvent equilibration run was followed by another 100 ps run without position restraints on the protein, in which all atoms were given an initial velocity obtained from a Maxwellian distribution at the desired initial temperature of 310 K.

A set of distance restraints was calculated from the X-ray structure of the isolated paddle (PDB code: 1ORS), using a cutoff of 1 nm. Only the S2–S4 portion was taken into account; the S1 helix in the isolated paddle structure is folded over S2, while in the full protein structure it forms an angle of approximately 120° and has contacts with the S2 helix of the neighboring subunit. This large difference in orientation of S1 might be due to the crystallization conditions, so we did not include the S1 portion in the calculation of the distance restraints. These distance restraints were applied in six successive MD simulations starting from the X-ray structure of the full protein, each 200 ps long. The force constants for the distance restraints were 10, 30, 100, 1000, 100 and 10 kJ mol^{-1} nm^{-2} for short-range interactions (distance detailed equilibrium simulations on this structure and the crystal structure are in preparation (K.M. Robertson et al.).

After building this model we performed a 10 ns steered MD simulation in which a force was applied to the tip of each paddle (residues 106–123), pulling them in the z direction towards the extracellular domain. A similar method has been used in studies of conformational changes in other proteins [22,23]. An ideal spring with a force constant of 3000 kJ mol^{-1} nm^{-2} was connected to the center of mass of the tip of each paddle and was moved in the direction parallel to the channel axis (z axis) at a rate of 0.25 nm/ns. Symmetry was not forced during the simulation, but the same set of distance restraints used to build the model was also applied during the steered MD simulation with a force constant of 200 kJ mol^{-1} nm^{-2} in order to avoid unfolding of the paddles. We also performed two additional steered MD simulations, using a reduced force constant of 50 kJ mol^{-1} nm^{-2} in the first and no distance restraints in the second; both showed substantial unfolding in the S4–S5 linker and in the S3a region, which is likely an artifact due to the high pull rate. In the present paper we will describe only the results of the steered MD with the higher force constant for the distance restraints.

2.2. Simulation details

All simulations were carried out using the GROMACS package version 3.1 [24,25], with the GROMOS87-based ffgmx forcefield and periodic boundary conditions. In GROMOS87 the energy of the interaction between single ions and carbonyl groups is underestimated [26], leading to artifacts in the simulation of ion permeation through ion channels. In simulations of KvAP using the standard GROMOS87 partial atomic charges we observed that all the potassium ions, initially placed in the selectivity filter, move to the bulk water within 2–5 ns. We reparameterized the partial charges on the carbonyl atoms of the four residues in the selectivity filter to give the correct interaction energy with potassium, based on the binding enthalpy of K^+ with N-methylacetamide (NMA) [26]; the values of 0.60 and

−0.60 elementary charges (for the carbon and the oxygen respectively) were found to reproduce the optimal cation–NMA interaction energy of 21.6 kcal/mol.

The simple point charge (SPC) water model was used [27]. The calculation of electrostatic forces utilized the PME implementation of the Ewald summation method [28,29]. The real space interactions were evaluated using a 0.9 nm cutoff and the reciprocal space interactions were evaluated on a 0.16 nm grid, using a fourth-order B-spline interpolation. A twin-range cutoff of 0.9–1.4 nm was used for the calculation of the van der Waals interactions. The protein, octane, and water were coupled separately to a temperature bath at 310 K with $\tau_T = 0.1$ ps using the Berendsen algorithm [30]. The pressure normal to the interface (z axis) was kept at 1 bar using weak pressure coupling with $\tau_P = 1.0$ ps [30], while the area in the xy plane was fixed. All bond lengths of non-water molecules were constrained with the LINCS algorithm [31], while the SETTLE algorithm was used to constrain bond lengths and angles in the water molecules [32]. Hydrogen atoms and the side chains of aromatic residues were replaced by dummy atom constructions, according to a published procedure, in order to remove these fast degrees of freedom from the system [33]. This allows a time step of 5 fs, with the neighbor list for the calculation of non-bonded interactions updated every four time steps. Coordinates of all atoms were sampled every 2 ps. Molecular graphics were created with the program VMD [34].

3. Results and discussion

3.1. Starting model

The starting structure for our simulation combines the structure of the full channel with the structure of the isolated paddle domain. Fig. 2 compares the crystal structure and our model structure. The root mean square deviation (RMSD) of the model structure from the crystallographic structure (calculated on the C-α carbons, after least square fit) is 0.74 nm for the whole protein. Comparing just the channel regions the RMSD is only 0.12 nm, while the paddles show an RMSD of 0.29 nm compared to the crystal structure of the isolated paddles. For comparison the RMSD between the S2–S4 domain in the full channel structure and in the isolated paddle structure is 0.67 nm. Helix S1 was not taken into account in the calculation of the RMSD, because its orientation with respect to S2–S4 in the isolated paddle structure is too different from its orientation in the full protein structure.

3.2. Effect of the pulling force on the pore region

During the simulation, the RMSD of the full protein relative to the X-ray structure increases almost linearly as the paddles are pulled towards the periplasmic side of the membrane. Despite the high pulling rate, however, the S5, S6 and pore helices are very stable, both in terms of RMSD (see Fig. 3) and of secondary structure (data not shown). The channel appears to be partially open in the starting structure, and the shape and the size of the pore undergo only minor modifications during the simulation (Fig. 4C,F). S6 shows little change, including around the conserved G220 residue that has been implicated in conformational change between the

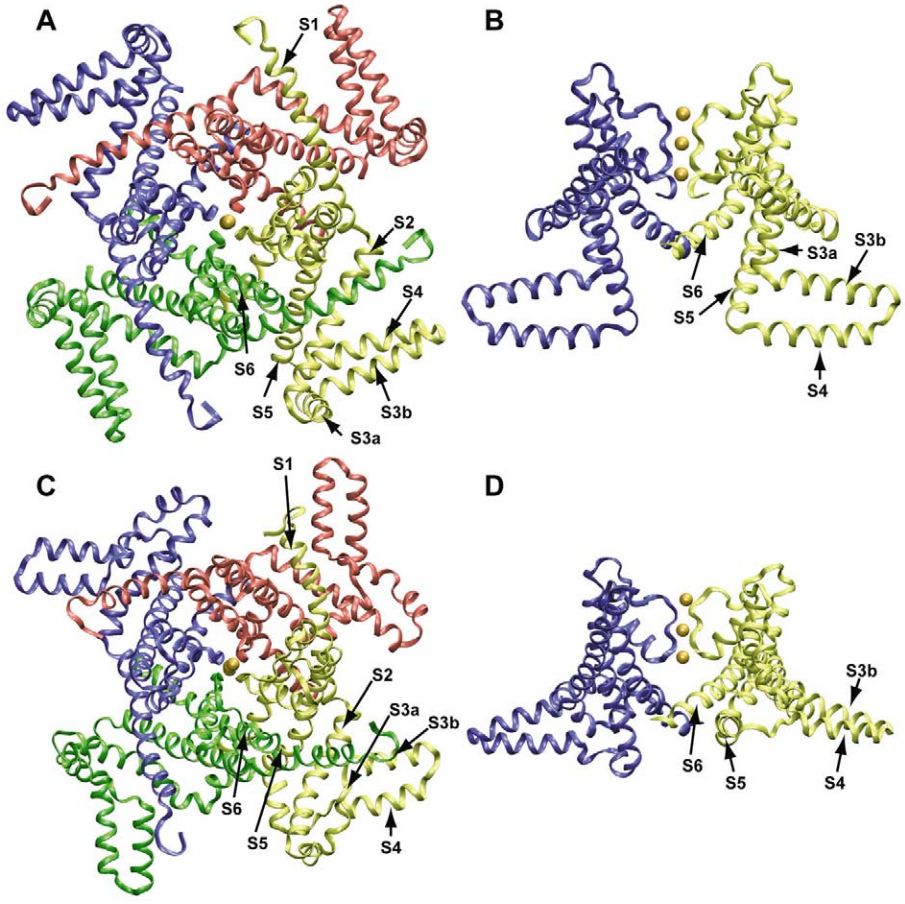

Fig. 2. Starting structure used for our simulations with a comparison to the X-ray structure of the full protein. The model was built starting from the crystal structure of the full protein and forcing the S2–S4 region of the voltage sensor region into a conformation similar to the crystal structure of the isolated paddle. The helices of monomer 1 (yellow) are labeled in each panel. A: Top view of crystal structure. B: Side view of crystal structure. C: Top view of the model. D: Side view of the model.

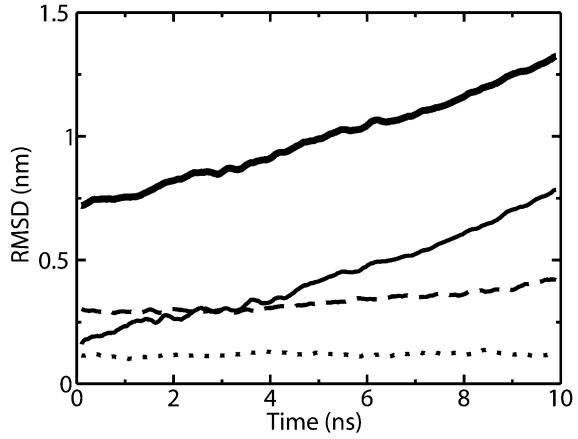

Fig. 3. RMSD during the steered MD simulation starting from our model. The RMSD was calculated on C-α carbons after least square fitting. Thick solid line: RMSD versus the crystal structure of the full protein (PDB code: 1ORQ); thin solid line: RMSD versus the starting structure of the model; dotted line: RMSD of the channel region (S6, P loop, selectivity filter and S5) versus the crystal structure of the full protein; dashed line: RMSD of the isolated voltage sensor (S1–S4) versus the crystal structure of the isolated paddle (PDB code: 1ORS).

open and closed states [35]. At the same time, the N-terminus of S5 and the S4–S5 linker show significant displacements, as highlighted in Fig. 4. The helical axis of the linker rotates about the channel axis by approximately 15–20° in all four monomers. The effect of the motion of the paddles is not propagated immediately – the opening of the channel would occur on a longer time scale. This might be reasonable as voltage gating can be described by a model that has four independent conformational changes, presumably the individual voltage sensors of each of the four domains, followed by a collective step that actually opens the channel [36].

In our starting model a salt bridge interaction between the side chains of K237 (close to the C-terminus of S6) and D146 (at the N-terminus of S5) is present although these residues are separated by about 1 nm (side chain–side chain) in the crystal structure. A similar interaction is seen in equilibrium simulations of this model in octane (10 ns, 20% of the time) and dimyristoyl-phosphatidylcholine (10 ns, 55% of the time), and to a lesser degree in 10 ns simulations of the crystal structure itself (Robertson et al., manuscript in preparation). Although these residues are not conserved in Kv channels, similar interactions might be involved in coupling S5 and S6 (Fig. 5). In addition to salt bridge interactions, K237 (located at the base of S6) interacts with the dipole of the S4–S5 linker. Interestingly, this is somewhat similar to the interaction between positively charged residues at the C-terminus of M2 that interact with the C-terminus of the slide helix in KirBac1.1 [10]. The importance of these residues could be tested by mutations, as they would be expected to have an effect on the gating characteristics of KvAP.

3.3. Effect of the pulling force on the paddle region

Secondary structure analysis shows that no major change occurs during the simulation. The S4–S5 linker and the S3a region show some partial unfolding, particularly at the ends. This is likely due to the high pulling rate. The RMSD of the paddle region increases only slightly during the simulation (Fig. 3). This can be explained in part by the application of distance restraints to the S2–S4 domain, which enforce the

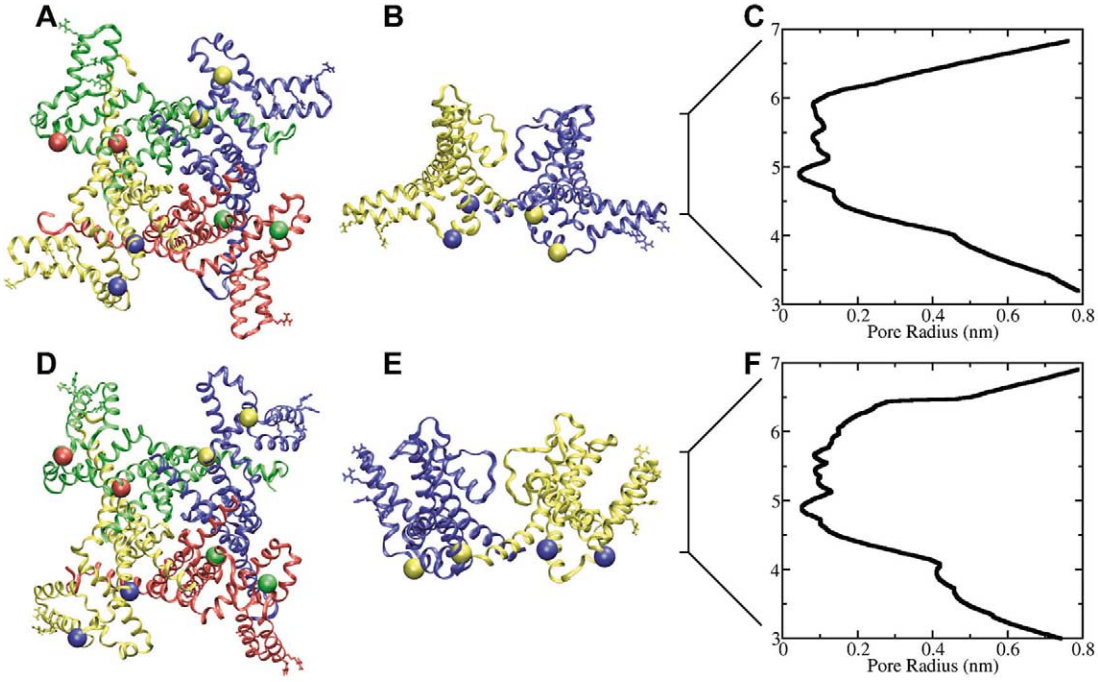

Fig. 4. Structures before (A–C) and after (D–F) pulling the tip of the paddle to the extracellular side of the protein. Views are shown from the cytoplasmic side (A,D) and from the plane of the membrane (B,E). Large spheres indicate the positions of the C-α carbon of residues S132 and K147 located near the ends of S4 and S5 respectively. As the paddle is pulled up, the S4–S5 linker moves in a clockwise direction (as viewed from the cytosol, A,D) and S132 moves from being below K147 to almost parallel (as viewed from the plane of the membrane, B,E). C,F show the radius of the central portion of the channel.

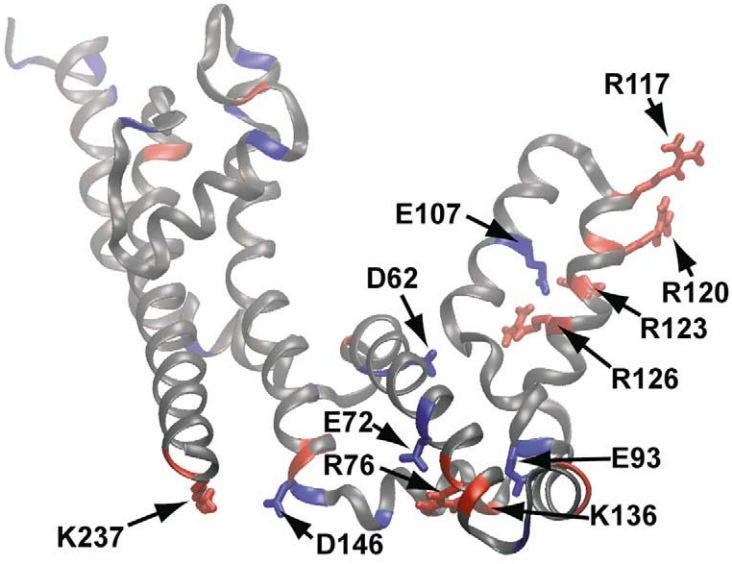

Fig. 5. Snapshot of a single subunit at time 9.5 ns. Residues are colored according to type: red, basic; blue, acidic; gray, neutral. Interactions that are proposed to play a role in the coupling between the motion of the paddles and the opening of the channel are highlighted. There is a hydrogen bond between the side chain of D62 and the backbone of G101 (not shown) at the bend between S3a and S3b. The salt bridge interaction between residue E93 and the backbone of K196 causes a rotation of S4 about its helical axis.

secondary but not the tertiary structure in helical regions. Visual inspection of the trajectory confirms that the paddles undergo mainly a rigid domain motion, with S2 acting as a hinge for the rotation of S3b and S4, in agreement with the suggestion of Jiang et al. [12].

Several stable hydrogen bonds and salt bridge interactions are observed during the simulation, both within the paddle and between the paddle and S2. Some of these are present in the crystal structure of the isolated paddle, while some others are unexpected. A hydrogen bond between the side chain of D62 (located in S2) and the backbone amide group of A100 is observed after building the model, and is also found in the X-ray structure of the isolated paddle (but not in structure of the full protein, in which S2 and S3b are far apart). During the simulation, the hydrogen bond shifts between A100 and G101; averaging over the four protein units, the latter is present in 81% of the simulation time and appears to be the only specific electrostatic interaction between S2 and S3a (see Fig. 5). Interestingly while neither A100 nor G101 is conserved, the highly conserved P99 causes a kink between helices S3a and S3b and exposes the backbone of A100 and G101 to hydrogen bonding with D62. Residue D62 is highly conserved in K^+ channels of both prokaryotic and eukaryotic species. This hydrogen bond would be expected to play a critical role in the first phase of the gating process, i.e. the motion of the paddles, allowing S2 to act as a hinge for the rotation of S3b and S4 if the paddle mechanism is correct.

Residues D72 and R76 (at the C-terminal end of S2) are also very conserved across species and may serve as a key to distinguish between different models. They form a very stable salt bridge throughout the simulation, which appears to stabilize the α-helical conformation of the C-terminal portion of S2 (see Fig. 5). The negatively charged E293 in Shaker (D72 in KvAP) contributes to the gating charge [37]. Both D72 and R76 move toward the cytosol as a result of the upward movement of the paddle. If the paddle model is correct, a mutation such as D72L or R76L would decrease or increase the gating charge respectively, while combining these mutations or a double mutation like D72R–R76D should recover the native gating charge.

Another two salt bridge interactions appear to play a role in restraining the motion of the paddles. They both involve the side chain of residue E93, located between S3a and S3b, which is highly conserved and known to play a role in the voltage-dependent gating. At the beginning of the simulation, E93 interacts mainly with R133, the C-terminal residue of helix S4. As the simulation proceeds, this electrostatic interaction with R133 weakens and is replaced by K136 (see Fig. 5). This interaction acts as a restraint for the motion of the paddles, which are forced to undergo a rotation about the helical axis of S3b; as a result of this rotation helix S4, which is closer than S3b to the intracellular solution at the beginning of the simulation (and in the crystal structure of the full protein), at the end is closer to the extracellular solution. The motion of the paddles is a combination of two rotations about two different hinges, namely S2 and the E93–K136 salt bridge (Fig. 1D). These observed rotations would be difficult to reconcile with the model of Fig. 1B because according to this model, S3b is not involved in the movement of the S4 helix. In addition, S4 does not appear to be close to S5 in the next unit, as suggested by the interpretation of mutagenesis and fluorescence data [17,38].

3.4. *Charges, solvation and ion pair interactions in the voltage sensor*

Both in the crystallographic structure of the full protein and in the starting structure of our model the five conserved arginine residues in the S4 helix (R117, R120, R123, R126, R133 in KvAP; R362, R365, R368, R371 and R377 in Shaker) are solvent exposed. As the simulation proceeds, S4 moves from the octane–water interface to the membrane-mimicking envi-

ronment. R117 enters the octane slab before the others, followed by R120, R123 and R126. The z coordinate of R133 shows little variation throughout the simulation, and therefore R133 seems to play a minor role in the gating charge, consistent with experimental results [39]. The exposed arginine side chains drag several hydrating water molecules with them into the octane slab. The presence of water in the interior of the hydrophobic medium is likely to be overestimated by our simulations. Due to the high pulling rate the intracellular water–octane interface does not truly reach equilibrium during the simulation, and the pockets of water in the proximity of the paddles remain connected to the bulk water in the intracellular space. After approximately 4 ns of simulation, the first four arginines are completely inserted into the octane slab, although they are still surrounded by water. Partial desolvation of R117 and R120 starts only 1.5 ns later, while R123 and R126 retain their full solvation shell until the end of the simulation (see Fig. 6).

The conformation of the helix-loop-helix motif formed by S3b and S4 appears to be stabilized by two salt bridge interactions involving E107 and two of the conserved arginines, R123 and R126; these contacts are observed for $\sim$95 and $\sim$35% of the simulation time respectively, with similar behavior in all four paddles. The R117 and R120 side chains do not have stable contacts with other protein residues. Since the water pockets surrounding the arginines are directly connected to the bulk water, chloride ions penetrate deep into the octane slab and form short-lived ion pairs with the positively charged side chains. Interestingly, the strength of the interaction with anions is different for each arginine residue; in particular, chloride ions have very weak interactions with R123 and R126, but much stronger interactions with R117 and R120. Averaging over the four protein units and over the whole trajectory, the ion pairs have a population of approximately 45% for R117 and of 40% for R120. The number of chloride ions interacting with the guanidinium groups increases during the simulations, starting from 0.1 ions per arginine and ending with $\sim$0.8 and $\sim$0.6 ions for R117 and R120 respectively. One possible explanation is that the hydrated chloride ions partially neutralize the high positive charge on S4, making it less difficult to cross the hydrophobic environment. A recent study has shown that polyarginine-based compounds show complex partitioning behavior in the presence of anions [40]. The observation of a solvent-accessible cavity in contact with the charged residues in S4 seems to be compatible with experimental results by Islas and Sigworth on the Shaker potassium channel [41], showing that the reduction of the ionic strength of the intracellular

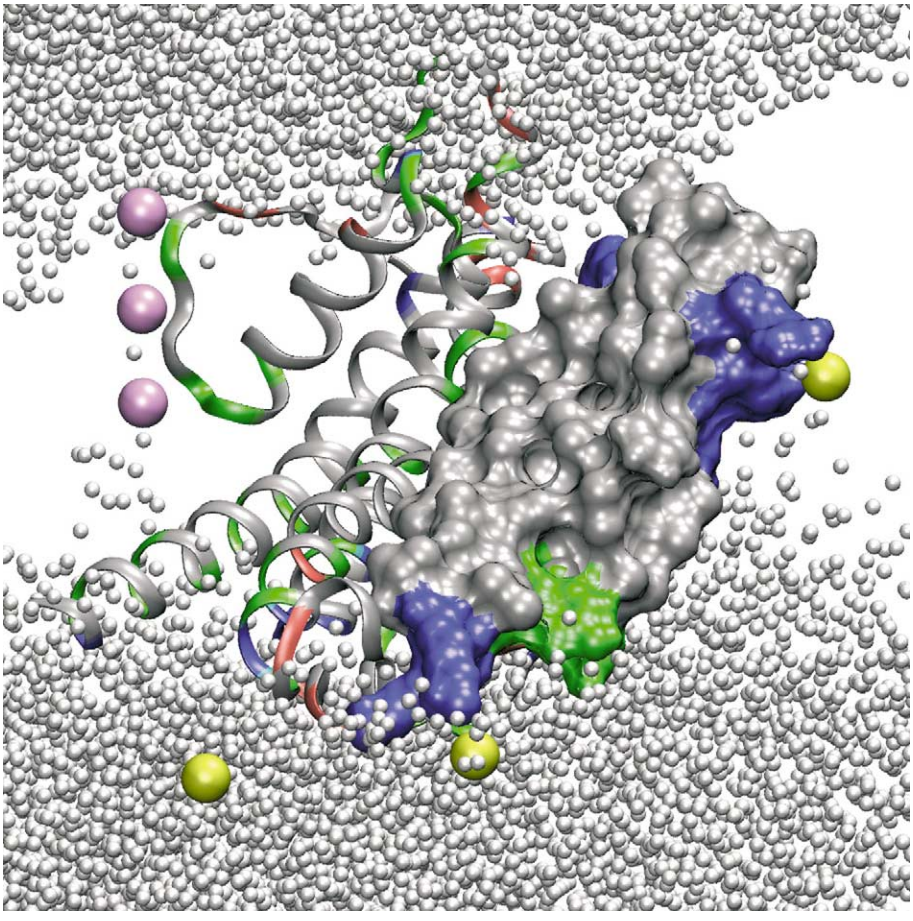

Fig. 6. Snapshot from the steered MD simulation (at time 9.5 ns). The residues are colored according to type: red, basic; blue, acidic; green, polar; gray, non-polar. The voltage-sensing paddle (S3b–S4) is shown as a surface representation. Water is shown as small white spheres; potassium is pink, and chloride is yellow. R117 and R120 share one solvated chloride ion, and drag substantially less water molecules into the membrane compared to R123 and R126.

solution (but not the extracellular) reduces the measured gating charge. They proposed, however, that S4 does not face the membrane but is located in a water-filled cavity shield from the membrane by S1–S3, consistent with several other models [42].

It is difficult to estimate the gating charge (the amount of charge that moves across the membrane and allows for the channel opening) from the simulation. The fifth conserved arginine in S4 seems to play a minor role; the charges on R123 and R126 seem to be partially neutralized by E107 (although there is also a rotation about the S3b axis, and therefore the z coordinate of the arginine residues changes more than that of the glutamate residue). Ion pairs are formed by R117 and R120, and all the charges appear to be solvated even in the middle of the octane layer, although this might be due to the high pulling rate. It would also be necessary to know the potential distribution, but this is likely to require a more accurate structure.

4. Conclusions

We have constructed a model of KvAP that combines the structure of the full-length protein with the high-resolution crystal structure of the paddle domain. After an initial relaxation we pulled the paddles through the membrane toward the periplasmic side to investigate the effect of this motion on the channel core and on the paddles. The pore region is remarkably stable during pulling and the shape of the channel opening and the structure of S5 and S6 do not significantly change during the pulling process on a 10 ns time scale. We have identified electrostatic interactions involving K237, D146 and the helix dipole of the S4–S5 linker that appear to couple motion of S5 to S6. A hydrogen bond between D62 in S2 and G101 in the paddle (made possible by the kink induced by P99) and a salt bridge between E93 and K136 might play pivotal roles in the motion of the paddles, in approximate agreement with the mechanism proposed by Jiang et al. [12]. If this mechanism is correct, it appears that the paddle has an additional rotation, as schematically shown in Fig. 1D. The structures obtained from the pulling process however are not easily reconciled with distance restraints based on the interpretation of crosslinking and cadmium binding sites as well as some accessibility studies. The exposed charges on S4 draw a considerable number of water molecules as well as chloride atoms into the membrane-like environment. Further calculations on simplified systems to investigate arginine partitioning into membranes in more detail with and without anions are underway. The significant amount of water and counter-ions that bind to S4 during insertion into the membrane make it difficult to estimate the energetic cost of such motions, as well as to estimate how much net charge is moving and what the potential distribution is. Further calculations are needed to shed more light on this.

Acknowledgements: DPT is a Scholar of the Alberta Heritage Foundation for Medical Research. This work was supported by the Canadian Institutes of Health Research. J.L.M. is supported by studentships from the Natural Sciences and Engineering Research Council and Alberta Ingenuity. L.M. thanks Dr. Giorgio Colombo, the Istituto di Chimica del Riconoscimento Molecolare-CNR (ICRM-CNR) and the Centre for biomolecular Interdisciplinary Studies and Industrial applications (CISI – University of Milan) for funding. Calculations were carried out in part on WestGrid facilities.

References

[1] Papazian, D.M., Schwarz, T.L., Tempel, B.L., Jan, Y.N. and Jan, L.Y. (1987) Science 237, 749–753.
[2] Hillle, B. (2001) Ion Channels of Excitable Membranes (3rd Edition), Sinauer Associates, Inc., Sunderland, MA.
[3] Yellen, G. (2002) Nature 419, 35–42.
[4] Sansom, M.S., Shrivastava, I.H., Bright, J.N., Tate, J., Capener, C.E. and Biggin, P.C. (2002) Biochim. Biophys. Acta 1565, 294–307.
[5] Roux, B. (2002) Curr. Opin. Struct. Biol. 12, 182–189.
[6] Bezanilla, F. and Perozo, E. (2003) Adv. Protein Chem. 63, 211–241.
[7] Doyle, D.A., Morais Cabral, J., Pfuetzner, R.A., Kuo, A., Gulbis, J.M., Cohen, S.L., Chait, B.T. and MacKinnon, R. (1998) Science 280, 69–77.
[8] Morais-Cabral, J.H., Zhou, Y. and MacKinnon, R. (2001) Nature 414, 37–42.
[9] Jiang, Y., Lee, A., Chen, J., Cadene, M., Chait, B.T. and MacKinnon, R. (2002) Nature 417, 523–526.
[10] Kuo, A. et al. (2003) Science 300, 1922–1926.
[11] Ruta, V., Jiang, Y., Lee, A., Chen, J. and MacKinnon, R. (2003) Nature 422, 180–185.
[12] Jiang, Y., Lee, A., Chen, J., Ruta, V., Cadene, M., Chait, B.T. and MacKinnon, R. (2003) Nature 423, 33–41.
[13] Laine, M., Lin, M.C., Bannister, J.P., Silverman, W.R., Mock, A.F., Roux, B. and Papazian, D.M. (2003) Neuron 39, 467–481.
[14] Jiang, Y., Ruta, V., Chen, J., Lee, A. and MacKinnon, R. (2003) Nature 423, 42–48.
[15] Miller, C. (2003) Nat. Struct. Biol. 10, 422–424.
[16] Cohen, B.E., Grabe, M. and Jan, L.Y. (2003) Neuron 39, 395–400.
[17] Broomand, A., Mannikko, R., Larsson, H.P. and Elinder, F. (2003) J. Gen. Physiol. 122, 741–748.
[18] Lee, H.C., Wang, J.M. and Swartz, K.J. (2003) Neuron 40, 527–536.
[19] Gonzalez, C., Rosenman, E., Bezanilla, F., Alvarez, O. and Latorre, R. (2001) Proc. Natl. Acad. Sci. USA 98, 9617–9623.
[20] Glauner, K.S., Mannuzzu, L.M., Gandhi, C.S. and Isacoff, E.Y. (1999) Nature 402, 813–817.
[21] Cha, A., Snyder, G.E., Selvin, P.R. and Bezanilla, F. (1999) Nature 402, 809–813.
[22] Grubmuller, H., Heymann, B. and Tavan, P. (1996) Science 271, 997–999.
[23] Tajkhorshid, E., Aksimentiev, A., Balabin, I., Gao, M., Isralewitz, B., Phillips, J.C., Zhu, F. and Schulten, K. (2003) Adv. Protein Chem. 66, 195–247.
[24] Berendsen, H.J.C., Vanderspoel, D. and Vandrunen, R. (1995) Comput. Phys. Commun. 91, 43–56.
[25] Lindahl, E., Hess, B. and van der Spoel, D. (2001) J. Mol. Model. 7, 306–317.
[26] Roux, B. and Berneche, S. (2002) Biophys. J. 82, 1681–1684.
[27] Berendsen, H.J.C., Postma, J.P.M., van Gunsteren, W.F. and Hermans, J. (1981) in: Intermolecular Forces (Pullman, B., Ed.), Reidel, Dordrecht.
[28] Essmann, U., Perera, L., Berkowitz, M.L., Darden, T., Lee, H. and Pedersen, L.G. (1995) J. Chem. Phys. 103, 8577–8593.
[29] Darden, T., York, D. and Pedersen, L. (1993) J. Chem. Phys. 98, 10089–10092.
[30] Berendsen, H.J.C., Postma, J.P.M., van Gunsteren, W.F., DiNola, A. and Haak, J.R. (1984) J. Chem. Phys. 81, 3684–3690.
[31] Hess, B., Bekker, H., Berendsen, H.J.C. and Fraaije, J. (1997) J. Comput. Chem. 18, 1463–1472.
[32] Miyamoto, S. and Kollman, P.A. (1992) J. Comput. Chem. 13, 952–962.
[33] Feenstra, K.A., Hess, B. and Berendsen, H.J.C. (1999) J. Comput. Chem. 20, 786–798.
[34] Humphrey, W., Dalke, A. and Schulten, K. (1996) J. Mol. Graph. 14, 33.
[35] Beckstein, O., Biggin, P.C., Bond, P., Bright, J.N., Domene, C., Grottesi, A., Holyoake, J. and Sansom, M.S. (2003) FEBS Lett. 555, 85–90.
[36] Horn, R. (2000) Biochemistry 39, 15653–15658.
[37] Seoh, S.A., Sigg, D., Papazian, D.M. and Bezanilla, F. (1996) Neuron 16, 1159–1167.

[38] Keynes, R.D. and Elinder, F. (1999) Proc. R. Soc. Lond. B Biol. Sci. 266, 843–852.
[39] Aggarwal, S.K. and MacKinnon, R. (1996) Neuron 16, 1169–1177.
[40] Sakai, N. and Matile, S. (2003) J. Am. Chem. Soc. 125, 14348–14356.
[41] Islas, L.D. and Sigworth, F.J. (2001) J. Gen. Physiol. 117, 69–89.
[42] Yang, N. and Horn, R. (1995) Neuron 15, 213–218.